LA-UR-16-23295
Approved for public release; distribution is unlimited.

Title: Dynamic System Simulation of the KRUSTY Experiment

Author(s): Klein, Steven Karl
Kimpland, Robert Herbert

Intended for: Report

Issued: 2016-05-09

Dynamic System Simulation of the KRUSTY Experiment

Steven K. Klein and Robert H. Kimpland
Advanced Nuclear Technology Group (NEN-2)
Los Alamos National Laboratory

Purpose

The proposed KRUSTY experiment is a demonstration of a reactor operating at power. The planned experimental configuration includes a highly enriched uranium (HEU) reflected core, cooled by multiple heat pipes leading to Stirling engines for primary heat rejection. Operating power is expected to be approximately four (4) to five (5) kilowatts with a core temperature above 1,000 K. No data is available on any historical reactor employing HEU metal that operated over the temperature range required for the KRUSTY experiment. Further, no reactor has operated with heat pipes as the primary cooling mechanism. Historic power reactors have employed either natural or forced convection so data on their operation is not directly applicable to the KRUSTY experiment.

In the absence of historical data, planning for the KRUSTY experiment must rely on modeling to estimate system performance across the entire set of operating conditions. However, the absence of this data suggests that the model itself cannot *a priori* be considered to accurately predict performance. Hence, initial models cannot appeal to data on historic reactors for validation; models will of necessity appeal to fundamental physics of the various subsystems comprising the configuration supplemented with any data available on the operation of these subsystems.

Three major subsystems may be recognized: (1) a nuclear element consisting of the HEU core, reflector, and shielding; (2) the heat pipes that will transfer heat from the core; (3) Stirling engines that will reject the heat transferred from the core by the heat pipes.

Experiments are planned by NASA to address the thermal characteristics of the heat pipes and the Stirling engines. Data arising from these experiments is expected to provide information that will assist in model refinement for these two subsystems. Critical experiments conducted as a prelude to operating the fully configured KRUSTY reactor at power would provide nuclear data needed to achieve the level of understanding necessary for the nuclear subsystem.

The primary purpose of the system model once developed and refined by data from these component experiments, will be used to plan the KRUSTY experiment. This planning will include expected behavior of the reactor from start-up, through various transient conditions where cooling begins to become present and effective, and finally establishment of steady-state. In addition, the model can provide indicators of anticipated off-normal events and appropriate operator response to those conditions. This information can be used to develop specific experiment operating procedures and aids to guide the operators in conduct of the experiment.

Introduction

As noted above, a physics model of the KRUSTY experiment has been developed. This model may be characterized as a dynamic system simulation (DSS) of the KRUSTY Experiment. The simulation model consists of a time-dependent "transient" model, which may be used to study both the steady-state and transient behavior of the system. The simulation model combines the point reactor kinetics model, which tracks the neutron behavior of the reactor, with a thermal-hydraulic model, which tracks the flow of heat in the reactor system. The system model includes the reactor core, sodium heat pipes, condenser plate, and Stirling engines. In addition, the corresponding frequency-dependent transfer functions of the simulation model have been generated to facilitate a linear stability analysis. Transfer functions for a one region fuel model and a multi-radial-region core, which tracks dynamic thermal profile of the core are both presented.

Any system component that directly contributes to reactivity feedback (i.e. possessing a reactivity feedback coefficient) or that significantly affects the temperature of such reactivity contributors needs to be included in the system model for completeness. The reactor neutron reflector is an example of the former, while the condenser plate, Stirling engines, and possibly the vacuum vessel are examples of the latter. At this point, the significance of these components is unclear. However, for completeness simple component models have been developed.

Point Reactor Kinetics Model

To track the neutronic behavior of the reactor the point reactor kinetics model is used. This model, in normalized form, is given by

$$\frac{dP_{fn}}{dt} = \frac{\beta}{\Lambda}\left[(R-1)P_{fn} + \sum_i F_i\, D_i\right]$$

and

$$\frac{dD_i}{dt} = \lambda_i\left(P_{fn} - D_i\right)$$

The total fission power deposited into the reactor core is given by

$$P_f = P_{fn}P_{fo}$$

Where

$P_{fo} =$ Initial reactor power

The reactivity model for the reactor with a single reactivity feedback mechanism (represented by the $\propto_T$ coefficient) due to fuel temperature, is given by

$$R = R_o + \propto_T \Delta T_f$$

Reactor Core Model

The reactor core, which consists of the highly enriched uranium (HEU) fuel rings, is described by a one-dimensional lumped parameter model in the radial direction. For N fuel lumps, the radial temperature of the fuel is given by

$$\frac{dT_{f,i}}{dt} = \frac{1}{M_{f,i}C_{pf}}\left(P_{f,i} + Q_{in,i} - Q_{out,i}\right), i = 1,2, \dots, N$$

Where

$T_{f,i}$ = fuel temperature in ith lump
$M_{f,i}$ = fuel mass in ith lump
C_{pf} = Specific heat of fuel
$P_{f,i}$ = fission energy deposited in ith lump

The flow of heat from one lump to another is given by simple conduction as

$$Q_{in,i,out,i} = -k_f A_{in,i,out,i}\frac{dT_{f,i}}{dr}$$

Where

k_f = thermal conductivity of the fuel
$A_{in,i,out,i}$ = heat transfer areas (in and out) of ith lump

The boundary conditions for the reactor core reflect the flow of heat across the innermost and outermost fuel lumps, given by

Core Boundary

$$Q_{in,1} = 0$$

$$Q_{out,N} = Q_{evap} + Q_{rad} = h_e A\_evap\left(T_{f,N} - T_s\right) + \frac{\sigma A_R\left({T_{f,N}}^4 - {T_{ves}}^4\right)}{\frac{1}{\varepsilon_f} + \frac{1}{\varepsilon_{ves}} + 1}$$

Where

h_e = heat pipe evaporator heat transfer coefficient
A_{evap} = heat pipe evaporator heat transfer area
T_s = Sodium vapor temperature
σ = Stefan-Boltzman constant
A_R = radial surface area of core
T_{ves} = heat shield/vacuum vessel temperature
ε_f = emissivity of fuel
ε_{ves} = emissivity of heat shield/vacuum vessel

Heat Pipes

Physical heat pipes are generally constructed of composite walls of different materials. In this case the actual temperature of the innermost region of the heat pipe is governed by heat conduction from the inner fuel surface through each wall material. Conduction through curved surfaces is generally described by the expression

$$Q = kA_m\Delta T$$

Where

A_m=log mean area of the curved surfaces: $A_m = \frac{A_o - A_i}{Ln\left(\frac{A_o}{A_i}\right)}$

k=overall heat transfer coefficient through the, j, composite regions with thickness t_j and individual heat transfer coefficient k_j: $\frac{1}{k} = \sum_j \frac{t_j}{k_j}$

At present, the heat flow from thermal radiation is neglected due to insufficient details on the experiment design; however, a preliminary treatment is presented later in this paper.

The system model for the sodium heat pipes consists of a single global sodium heat pipe. In the form of a single lump, this global heat pipe has the geometric characteristics of the sum of all the actual heat pipes. Heat transfer from the global heat pipe to the condenser plate is given by

$$Q_{con} = h_c A_{con}(T_s - T_c)$$

Where

h_c = heat pipe condenser heat transfer coefficient
A_{con} = heat pipe condenser heat transfer area
T_c = condenser plate temperature

The saturation temperature of the Sodium vapor as a function of vapor pressure is given by

$$T_s = \frac{2C_3}{(-C_2 + (C_2C_2 + 4C_1C_3 - 4C_3\ln(P))^{0.5})}$$

C_1, C_2, and C_3 are geometric correction factors for surface heat flux and the boiling limit. These factors depend on the particular heat pipe geometry and fluid. For a cylindrical heat pipe with Na working fluid they may take the form:

$$C_1 = -\frac{t_{wick}}{r_o ln\left(1 - \frac{t_{wick}}{r_o}\right)};\ C_2 = \frac{r_o}{r_i};\ C_3 = \frac{0.5}{r_{ne}}$$

Where

t_{wick} =wick thickness
r_o = outer radius of the working region of the heat pipe
r_i = inner radius
r_{ne} = radius of nucleation sites in microns.

The Sodium vapor pressure is given by

$$\frac{dP}{dt} = \frac{dm}{dt}\left(\frac{R_g T_s}{V}\right)$$

Where

$m =$ mass of Sodium vapor
$R_g =$ Sodium vapor gas constant
$V =$ volume of Sodium vapor

The Sodium vapor mass flow rate is given by

$$\frac{dm}{dt} = \left(\frac{Q_{evap} - Q_{con}}{h_{fg}}\right)$$

Where

$h_{fg} =$ Sodium latent heat of vaporization

Heat Pipe Heat Transfer Coefficients

For the heat pipes, heat transfer coefficients are modeled as simple thermal resistances based on the thickness of the Sodium liquid layer. These resistances are given by

$$h_c A_{con} = \frac{2\pi l_c k_l}{\ln \frac{r_o}{r_i}}$$

And

$$h_e A_{evap} = \frac{2\pi l_e k_l}{\ln \frac{r_o}{r_i}}$$

Where

$l_c =$ length of the condenser
$l_e =$ length of the evaporator
$k_l =$ thermal conductivity of Sodium liquid
$r_o =$ Sodium liquid outer radius
$r_i =$ Sodium liquid inner radius

The heat transfer coefficient between the condenser plate and the Stirling engine will probably take the form of a convective heat transfer coefficient. The hydraulic diameter of the engine is given by

$$d = \frac{4V_{he}}{A_w}$$

Where

V_{he} = volume of engine's heat exchanger
A_w = wetted area of heat exchanger

The Reynold's number for the engine's heat exchanger working fluid is given by

$$Re = \frac{\rho u d}{\mu}$$

Where

ρ = working fluid density
u = working fluid bulk velocity
μ = working fluid dynamic viscosity

The corresponding Nusselt number for this situation would be given by

$$Nu = \frac{h_n d}{k}$$

Where

k = thermal conductivity of the working fluid

Given the geometry of the engine's heat exchanger and the speed of the engine (frequency), the above parameters would be calculated assuming quasi-steady flow conditions. Generally, the engine's heat transfer coefficient would be calculated using a semi-empirical correlation that gives the Nusselt number as a function of the working fluid's Reynold's and Prandtl numbers.

Example of Model Results

Consider a notional annular core composed of HEU and 8% Molybdenum (U-8Mo). The heat pipes are assumed to be eight in number and cylindrical with a composite wall consisting of Molybdenum in contact with the HEU core and inner layers of Haynes 230 stainless steel and Sodium. An MCNP model was developed to obtain nuclear parameters such as the mean-neutron-generation-time, prompt neutron fraction, core averaged temperature coefficient of reactivity, and flux distribution by radial region.

Due to the uncertainties in actual geometries and equipment parameters described above presentation of actual dimensions used is suppressed; hence, overall general operational characteristics are reported.

Figure 1 presents model representation of the first 1,000 seconds of a $1.00 reactivity insertion at a rate of $0.1/sec while Figure 2 is a detail of the first 100 seconds of the event. In these figures the core dynamics typical of a reactivity insertion into an HEU core can be seen. Fission Power rises sharply with the insertion and is quenched by the advent of heat removal. The various temperature traces are of fuel regions (T1, T5, T10; inner to outer) and the heat pipe Sodium vapor temperature, Ts. The close coupling

of thermal behavior in the core and heat pipes can be seen. Quasi-steady-state is reached by the end of the model run.

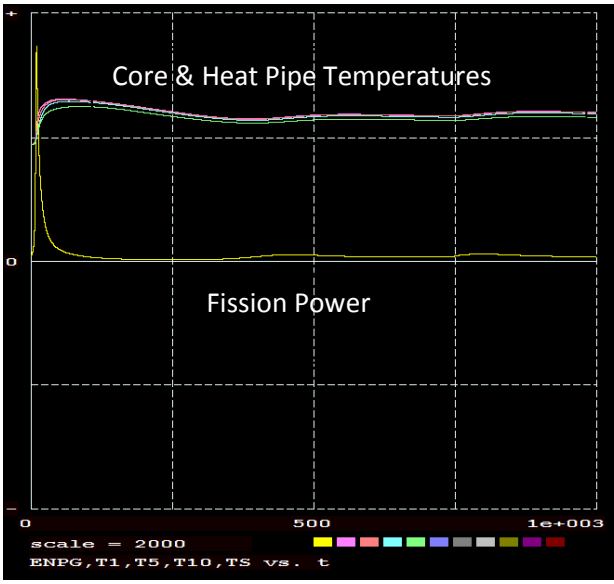

Figure 1 $1.00 Reactivity Insertion

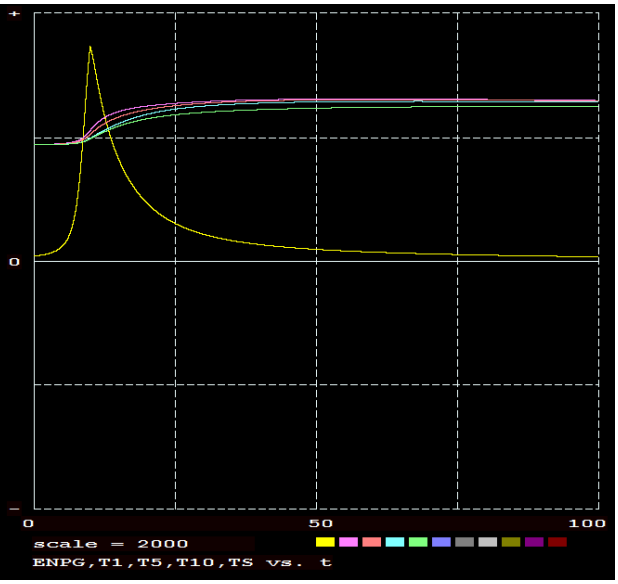

Figure 2 $1.00 Insertion Detail

Figure 3 presents the results of a $3.00 reactivity insertion. In this case heat removal starts prior to full reactivity insertion so system response exhibits more features; however, once full reactivity insertion occurs steady-state quickly ensues. This response can be seen in Figure 4 where an additional $0.50 step reactivity insertion occurs once steady-state is reached form the initial case. Here, again, a new steady-state operating position is reached.

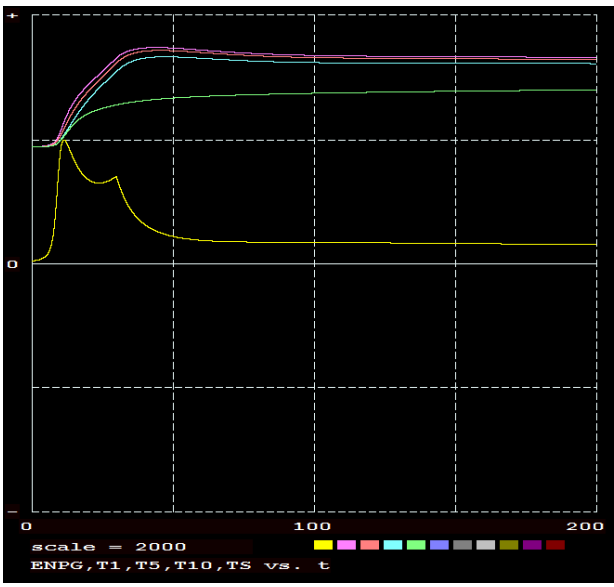

Figure 3 $3.00 Reactivity Insertion

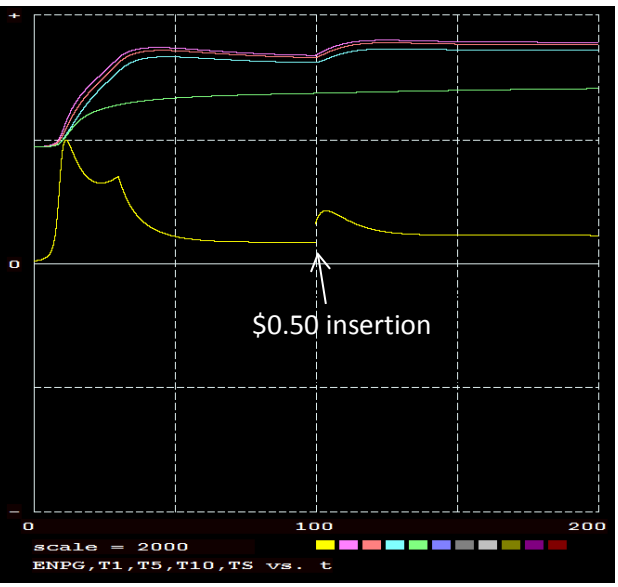

Figure 4 $0.50 Step Insertion

As can be seen from Figure 4 the DSS model is capable of estimating response to dynamic events at any point in the system timeline. Examples of typical events of interest are shown in Figures 5 and 6.

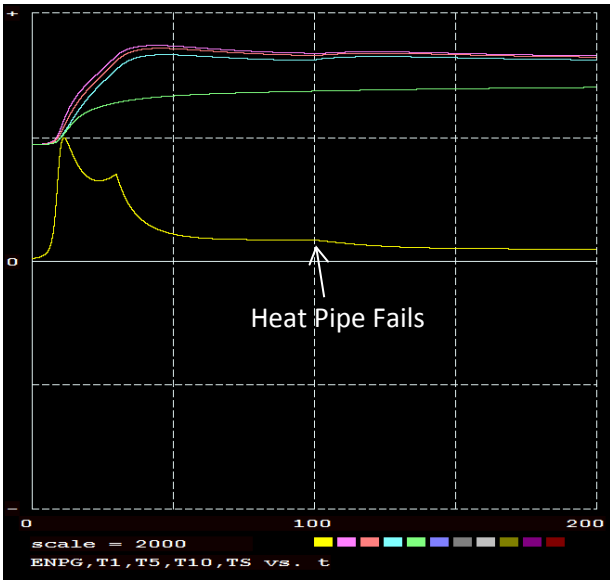

Figure 5 $3.00 Loss of Single Heat Pipe

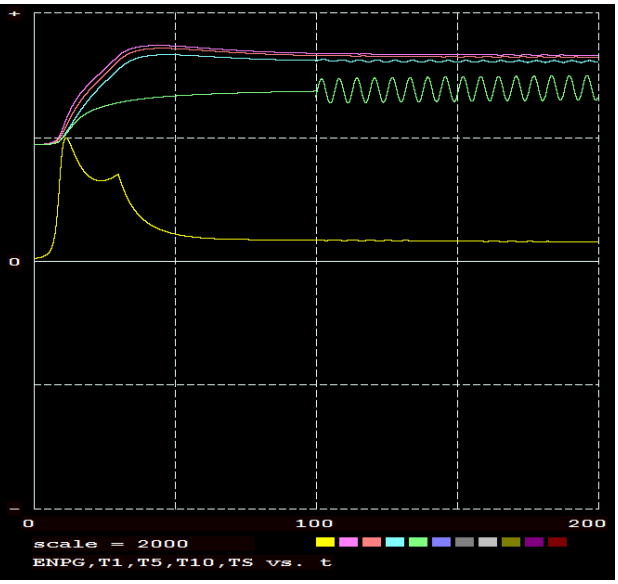

Figure 6 Saturation Temperature Oscillation

As noted previously, actual values are suppressed due to stated uncertainties; however, the general characteristics of system dynamics are typical of an HEU core with heat removal.

Linear Stability Model

The time-dependent model presented above was linearized and transformed into the frequency domain with the use of Laplace transforms. To facilitate the development of closed loop and open loop transfer functions, both a single and a multi-region core model were developed.

One region fuel model

The one region fuel model is described as follows

$$\frac{dT_f}{dt} = \frac{1}{M_f C_{pf}}\left(P_f - h_e A_{evap}(T_f - T_s)\right)$$

Where

M_f = total fuel mass
P_f = total fission power deposited in the fuel

This one region model leads to the following set of characteristic time constants

$$g_1 = \frac{h_e A_{evap} R_g}{h_{fg} V}\,;\, g_2 = \frac{h_c A_{con} R_g}{h_{fg} V}\,;\, g_3 = \frac{1}{M_f C_{pf}}\,;\, g_4 = \frac{h_e A_{evap}}{M_f C_{pf}}$$

$$W = -c_2 + (c_2^2 + 4c_1c_3 - 4c_3\ln(P_o))^{0.5}\,;\, U = c_2^2 + 4c_1c_3 - 4c_3\ln(P_o)\,;\, Y = \frac{4c_3^2}{P_o W^2 U^{0.5}}$$

The one region fuel temperature transfer function is given by

$$\tilde{T}_f = \frac{g_3 \tilde{P}_f}{\left[s + g_4 - \frac{T_{so} Y g_1 g_4}{s\left(1 - \frac{Y\left(g_1 T_{fo} - 2g_1 T_{so} - 2g_2 T_{so} + g_2 T_c\right)}{s}\right)} \right]}$$

The typical forward transfer function based on the point reactor kinetics model is given by

$$G_1 = \left(\frac{\tilde{P}_f}{\tilde{R}}\right) = \frac{P_{fo}}{\left[\frac{\Lambda}{\beta} s + \sum_{k=1}^{m} \frac{F_k s}{s + \lambda_k}\right]}$$

Where

P_{fo} = steady-state power
F_k = delayed neutron precursor fraction
λ_k = delayed neutron precursor time constant
$\frac{\Lambda}{\beta}$ = inverse rossi-alpha value

For a single reactivity feedback mechanism of fuel temperature change, the feedback transfer function is given by

$$H = \left(\frac{\tilde{R}}{\tilde{P}_f}\right) = \frac{\propto_T g_3}{\left[s + g_4 - \frac{T_{so} Y g_1 g_4}{s\left(1 - \frac{Y\left(g_1 T_{fo} - 2g_1 T_{so} - 2g_2 T_{so} + g_2 T_c\right)}{s}\right)} \right]}$$

Where

$\propto_T = |\propto_T|$ = fuel temperature reactivity feedback coefficient

The closed loop transfer function is given by

$$G_{cl} = \frac{G_1}{1 + G_1 H}$$

The open loop transfer function is given by

$$G_{ol} = G_1 H$$

With these derivations traditional graphical representations may be developed including Nyquist Plot (Figure 7), Nichols Plot (Figure 8), Bode Amplitude and Frequency Plots (Figures 10 and 11). Internal functions in *Mathematica* were used to generate these plots.

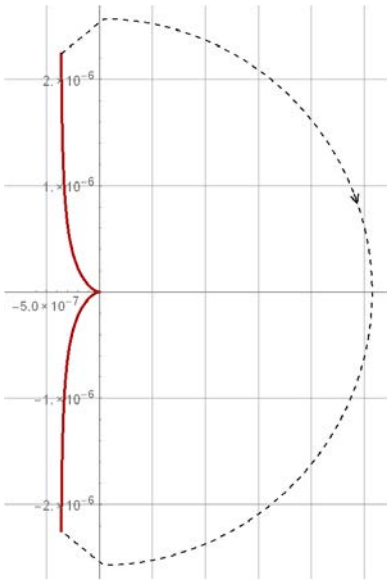

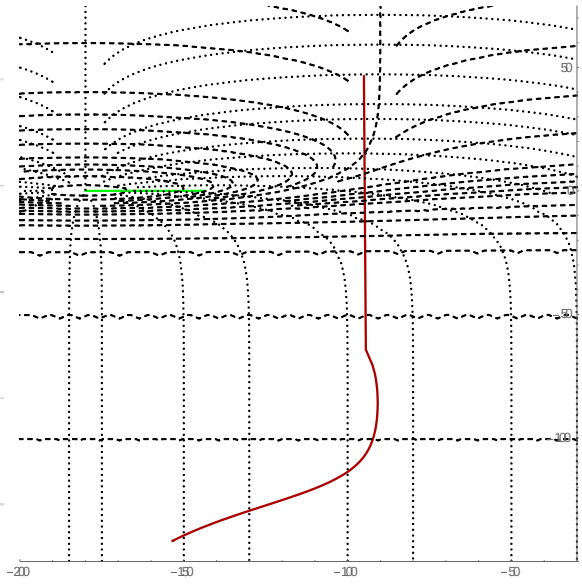

Figure 7 Single Region Core Nyquist Plot Figure 8 Single Region Core Nichols Plot

Both the Nyquist and Nichols plots show a phase stability margin of approximately -100°.

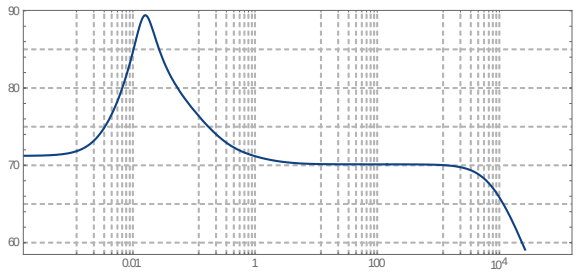

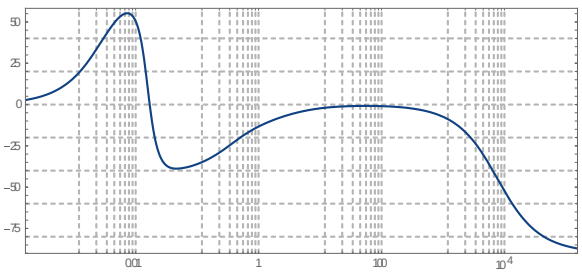

Figure 9 Single Region Core Bode Amplitude Plot Figure 10 Single Region Core Bode Frequency Plot

Bode plots exhibit no discontinuities or other anomalies along with some resonance regions.

Multi-region Core Model

The multi-region core model is given by

$$\frac{dT_{f,i}}{dt} = \frac{1}{M_{f,i}C_{pf}}\left(P_{f,i} + Q_{in,i} - Q_{out,i}\right), i = 1,2,\dots,N$$

Where the heat flows from one fuel lump to the next is given by

$$Q_{in,i} = k_f A_{in,i}(T_{f,i-1} - T_{f,i})/dr$$

and

$$Q_{out,i} = k_f A_{out,i}(T_{f,i} - T_{f,i+1})/dr$$

Where

$dr =$ radial thickness of a fuel lump

The fission energy deposited into each lump is given by

$$P_{f,i} = FRA_i P_f$$

Where

$FRA_i =$ fraction of total fission energy deposited into ith region

The following set of system time constants characterize the multi-region model transfer functions for a ten region core model.

$$g_1 = \frac{h_e A_{out10} R_g}{h_{fg} V} ; g_2 = \frac{h_c A_{con} R_g}{h_{fg} V}$$

$$g_{101} = FRA_{10}/M_{f10}/C_{pf} ; g_{102} = k_f A_{in10}/dr/M_{f10}/C_{pf}$$

$$g_{103} = k_f A_{in10}/dr/M_{f10}/C_{pf} + h_e A_{out10}/M_{f10}/C_{pf} ; g_{104} = h_e A_{out10}/M_{f10}/C_{pf}$$

$$W = -c_2 + (c_2^2 + 4c_1c_3 - 4c_3\ln(P_o))^{0.5} ; U = c_2^2 + 4c_1c_3 - 4c_3\ln(P_o) ; Y = \frac{4c_3^2}{P_o W^2 U^{0.5}}$$

$$g_{105} = \frac{T_{so} Y g_1}{s\left(1 - \frac{Y(g_1 T_{f10o} - 2g_1 T_{so} - 2g_2 T_{so} + g_2 T_c)}{s}\right)}$$

$$g_{91} = FRA_9/M_{f9}/C_{pf} ; g_{92} = k_f A_{in9}/dr/M_{f9}/C_{pf} ; g_{93} = k_f A_{in9}/dr/M_{f9}/C_{pf} + g_{92}$$

$$g_{84} = k_f A_{out8}/M_{f8}/C_{pf} ; g_{71} = FRA_7/M_{f7}/C_{pf}$$

$$g_{72} = k_f A_{in7}/dr/M_{f7}/C_{pf} ; g_{73} = k_f A_{in7}/dr/M_{f7}/C_{pf} + g_{72}$$

$$g_{74} = k_f A_{out7}/M_{f7}/C_{pf} ; g_{61} = FRA_6/M_{f6}/C_{pf}$$

$$g_{62} = k_f A_{in6}/dr/M_{f6}/C_{pf} ; g_{63} = k_f A_{in6}/dr/M_{f6}/C_{pf} + g_{62}$$

$$g_{64} = k_f A_{out6}/M_{f6}/C_{pf} ; g_{51} = FRA_5/M_{f5}/C_{pf}$$

$$g_{52} = k_f A_{in5}/dr/M_{f5}/C_{pf} ; g_{53} = k_f A_{in5}/dr/M_{f5}/C_{pf} + g_{52}$$

$$g_{54} = k_f A_{out5}/M_{f5}/C_{pf} ; g_{41} = FRA_4/M_{f4}/C_{pf}$$

$$g_{42} = k_f A_{in4}/dr/M_{f4}/C_{pf} ; g_{43} = k_f A_{in4}/dr/M_{f4}/C_{pf} + g_{42}$$

$$g_{44} = k_f A_{out4}/M_{f4}/C_{pf} ; g_{31} = FRA_3/M_{f3}/C_{pf}$$

$$g_{32} = k_f A_{in3}/dr/M_{f3}/C_{pf} ; g_{33} = k_f A_{in3}/dr/M_{f3}/C_{pf} + g_{32}$$

$$g_{34} = k_f A_{out3}/M_{f3}/C_{pf}\ ;\ g_{21} = FRA_2/M_{f2}/C_{pf}$$

$$g_{22} = k_f A_{in2}/dr/M_{f2}/C_{pf}\ ;\ g_{23} = k_f A_{in2}/dr/M_{f2}/C_{pf} + g_{22}$$

$$g_{24} = k_f A_{out2}/M_{f2}/C_{pf}\ ;\ g_{11} = FRA_1/M_{f1}/C_{pf}\ ;\ g_{14} = k_f A_{out1}/M_{f1}/C_{pf}$$

The following algebraic expressions involve the various g_{ij} values just defined

$$A_9 = \frac{g_{91}+\frac{g_{94}g_{101}}{s+g_{103}-g_{104}g_{105}}}{s+g_{93}-\frac{g_{94}g_{102}}{s+g_{103}-g_{104}g_{105}}}\ ;\ B_9 = \frac{g_{92}}{s+g_{93}-\frac{g_{94}g_{102}}{s+g_{103}-g_{104}g_{105}}}$$

$$A_8 = \frac{g_{81}+g_{84}A_9}{s+g_{83}-g_{84}B_9}\ ;\ B_8 = \frac{g_{82}}{s+g_{83}-g_{84}B_9}$$

$$A_7 = \frac{g_{71}+g_{74}A_8}{s+g_{73}-g_{74}B_8}\ ;\ B_7 = \frac{g_{72}}{s+g_{73}-g_{74}B_8}$$

$$A_6 = \frac{g_{61}+g_{64}A_7}{s+g_{63}-g_{64}B_7}\ ;\ B_6 = \frac{g_{62}}{s+g_{63}-g_{64}B_7}$$

$$A_5 = \frac{g_{51}+g_{54}A_6}{s+g_{53}-g_{54}B_6}\ ;\ B_5 = \frac{g_{52}}{s+g_{53}-g_{54}B_6}$$

$$A_4 = \frac{g_{41}+g_{44}A_5}{s+g_{43}-g_{44}B_5}\ ;\ B_4 = \frac{g_{42}}{s+g_{43}-g_{44}B_5}$$

$$A_3 = \frac{g_{31}+g_{34}A_4}{s+g_{33}-g_{34}B_4}\ ;\ B_3 = \frac{g_{32}}{s+g_{33}-g_{34}B_4}$$

$$A_2 = \frac{g_{21}+g_{24}A_3}{s+g_{23}-g_{24}B_3}\ ;\ B_2 = \frac{g_{22}}{s+g_{23}-g_{24}B_3}$$

$$A_1 = \frac{g_{11} + g_{14}A_2}{s + g_{14} - g_{14}B_2}$$

A final set of algebraic expressions are accumulations of the A_i, and B_j values

$$C_4 = \Big(A_4 + B_4\big(A_3 + B_3(A_2 + B_2A_1)\big)\Big)\ ;\ C_6 = \big(A_6 + B_6(A_5 + B_5C_4)\big)\ ;\ C_8 = \big(A_8 + B_8(A_7 + B_7C_6)\big)$$

These expressions are used in preparing the multi-region fuel temperature transfer functions

$$\tilde{T}_{f1} = A_1\tilde{P}_f\ ;\ \tilde{T}_{f2} = (A_2 + B_2A_1)\tilde{P}_f\ ;\ \tilde{T}_{f3} = (A_3 + B_3(A_2 + B_2A_1))\tilde{P}_f\ ;\ \tilde{T}_{f4} = C_4\tilde{P}_f$$

$$\tilde{T}_{f5} = (A_5 + B_5C_4)\tilde{P}_f\ ;\ \tilde{T}_{f6} = C_6\tilde{P}_f\ ;\ \tilde{T}_{f7} = (A_7 + B_7C_6)\tilde{P}_f\ ;\ \tilde{T}_{f8} = C_8\tilde{P}_f$$

$$\tilde{T}_{f9} = (A_9 + B_9C_8)\tilde{P}_f\ ;\ \tilde{T}_{f10} = \frac{g_{101}+g_{102}(A_9+B_9C_8)}{s+g_{103}-g_{104}g_{105}}\tilde{P}_f$$

As for the single region treatment expressions for reactivity and average fuel temperature are required

The multi-region reactivity model is given by

$$R = R_o + \alpha_T(T_{fav} - T_{fo})$$

Where the average fuel temperature is given by

$$T_{fav} = \sum_i^N \frac{M_{fi}T_{fi}}{\sum_i^N M_{fi}}$$

Thus, the reactivity transfer function is given by

$$\tilde{R} = \alpha_T \sum_i^N \frac{M_{fi}\tilde{T}_{fi}}{\sum_i^N M_{fi}}$$

The multi-region feedback transfer function is given by

$$H_{mr} = \left(\frac{\tilde{R}}{\tilde{P}_f}\right) = \alpha_T \sum_i^N \frac{M_{fi}\frac{\tilde{T}_{fi}}{\tilde{P}_f}}{\sum_i^N M_{fi}}$$

Where

$$\propto_T = |\propto_T|$$

Again, the forward transfer function is given by

$$G_1 = \left(\frac{\tilde{P}_f}{\tilde{R}}\right) = \frac{P_{fo}}{\left[\frac{\Lambda}{\beta}s + \sum_{k=1}^m \frac{F_k s}{s+\lambda_k}\right]}$$

And the closed loop transfer function is

$$G_{cl} = \frac{G_1}{1 + G_1 H_{mr}}$$

And the open loop transfer function by

$$G_{ol} = G_1 H_{mr}$$

These expressions allow generation of linear stability plots. As was the case for the single region model internal functions in *Mathematica* were used to generate these plots presented in Figures 11 through 14.

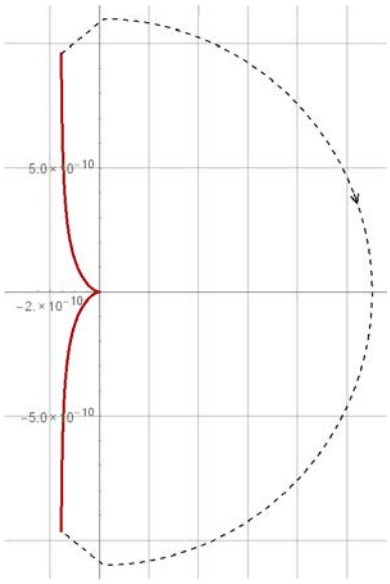

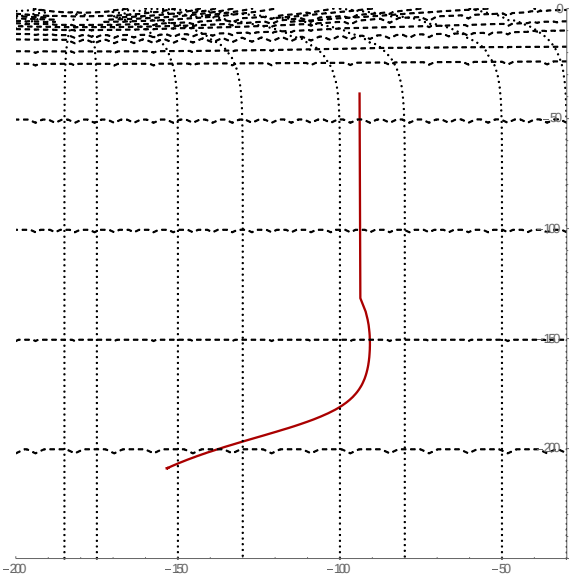

Figure 11 Multi-Region Core Nyquist Plot Figure 12 Multi-Region Core Nichols Plot

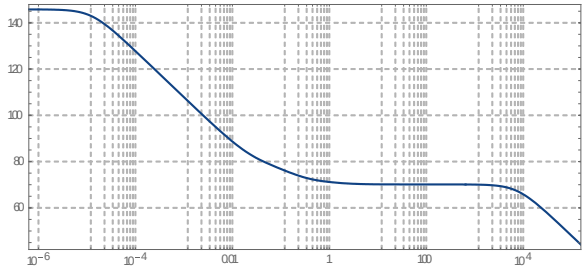

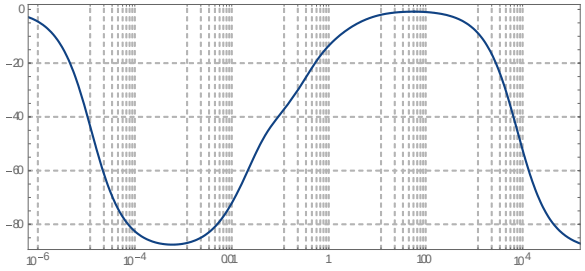

Figure 13 Multi-Region Core Bode Amplitude Plot Figure 14 Multi-Region Core Bode Frequency Plot

Comparison of Figures 8 through 10 with Figures 11 through 14 show nearly identical agreement in form with some frequency shift in the Bode plots.

The other necessary Nyquist criterion is that there are no positive poles. Table 1 provides the full (non-zero) poles of the open loop transfer function:

Table 1 Poles of the single region core open loop transfer function

(7,718.08)	(1,126.55)	(1,126.55)	(1,126.55)	(1,126.55)	(1,126.55)	(1,126.55)	(1,126.55)	(1,126.55)	(1,126.55)
(1,126.55)	(2.8982)	(1.0241)	(0.4853)	(0.4848)	(0.4664)	(0.3645)	(0.3641)	(0.3641)	(0.3640)
(0.3629)	(0.3602)	(0.3556)	(0.3473)	(0.3434)	(0.3421)	(0.3420)	(0.3415)	(0.3363)	(0.3301)
(0.3253)	(0.3116)	(0.3096)	(0.3095)	(0.3085)	(0.3079)	(0.2967)	(0.2863)	(0.2785)	(0.2753)
(0.2729)	(0.2719)	(0.2714)	(0.2695)	(0.2511)	(0.2444)	(0.2439)	(0.2378)	(0.2332)	(0.2305)
(0.2275)	(0.2269)	(0.2236)	(0.2230)	(0.2089)	(0.2027)	(0.1991)	(0.1975)	(0.1969)	(0.1966)
(0.1948)	(0.1906)	(0.1837)	(0.1793)	(0.1762)	(0.1756)	(0.1755)	(0.1755)	(0.0682)	(0.0143)
(0.0107)									

Examination of these plots and poles allow the following observations and conclusions:

- Bethe Criteria – No infinite resonance in Bode Plots
- Nyquist Criteria – Number of clockwise encirclements of 1- plus the number of right hand plane poles is zero (transfer function has no positive poles)
- Nichols Criteria – One sheeted full Nichols plot of the transfer function does not intersect the point (-180, 0 db)

The Nyquist and Nichols Criteria conclusions are necessary and sufficient to establish stability of the model in the linear approximation. The Bethe criterion is necessary for non-linear system stability.

Expanded Model Components

The reflector and condenser plate are additional components that contribute to the overall performance of the system.

Reflector Model

The radial reflector, which is located outside the vacuum vessel, may or may not have an associated cooling system. The reflector model presented below uses a once-through cooling system to cool the reflector. The radial reflector temperature is given by

$$\frac{dT_R}{dt} = g_{1R}P_f - g_{2R}(T_R - C_1)$$

Where

$$g_{1R} = \frac{FRA_R}{M_R C_{pR}}; g_{2R} = \frac{h_R A_{ref}}{M_R C_{pR}}$$

And

FRA_R = scaling factor between core and reflector power
M_R = reflector mass
C_{pR} = specific heat of reflector
h_R = heat transfer coefficient between reflector and coolant
A_{ref} = reflector heat transfer area

The average temperature of the coolant is given by

$$\frac{dC_1}{dt} = g_{3R}(C_{in} - C_1) + g_{4R}(T_R - C_1)$$

The output temperature of the coolant is given by

$$\frac{dC_2}{dt} = g_{3R}(C_1 - C_2) + g_{4R}(T_R - C_1)$$

Where

$$g_{3R} = \frac{2W_C}{M_C}; g_{4R} = \frac{h_R A_{ref}}{M_C C_{pC}}$$

and

W_C = coolant mass flow rate
M_C = coolant mass
C_{pC} = specific heat of coolant

The transfer function for the reflector temperature is then given by

$$\tilde{T}_R = \frac{g_{1R}\tilde{P}_f}{s + g_{2R} - \frac{g_{2R}g_{4R}}{s + g_{3R} + g_{4R}}}$$

Condenser Plate

The condenser plate serves as the heat sink for the heat pipes and the heat source for the Stirling engines. The time-dependent condenser temperature model is given by

$$\frac{dT_c}{dt} = g_{1E}(T_S - T_C) - g_{2E}(T_C - T_E)$$

Where

$$g_{1E} = \frac{h_c A_{con}}{M_{con} C_{pcon}}; g_{2E} = \frac{h_n A_n}{M_{con} C_{pcon}}$$

And

M_{con} = mass of condenser plate
C_{pcon} = specific heat of condenser plate
h_n = heat transfer coefficient between condenser plate and Stirling engines
A_n = heat transfer area between condenser plate and stirling engines
T_E = upper temperature of stirling engine

The transfer function for the condenser plate temperature is then given by

$$\tilde{T}_C = \frac{g_{1E}\tilde{T}_S}{s + g_{1E} + g_{2E}}$$

The time-dependent condenser plate temperature leads to the following modifications of the previously described linear stability model.

$$g_{3E} = \frac{g_2 T_{so} g_{1E}}{s + g_{1E} + g_{2E}}$$

One region model

$$\tilde{T}_f = \frac{g_3 \tilde{P}_f}{\left[s + g_4 - \frac{T_{so} Y g_1 g_4}{s\left(1 - \frac{Y\left(g_1 T_{fo} - 2g_1 T_{so} - 2g_2 T_{so} + g_2 T_{co} + g_{3E}\right)}{s}\right)} \right]}$$

Multi-region model

$$g_{105} = \frac{T_{so} Y g_1}{s\left(1 - \frac{Y\left(g_1 T_{f10o} - 2g_1 T_{so} - 2g_2 T_{so} + g_2 T_{co} + g_{3E}\right)}{s}\right)}$$

Expanded Model Stability

The transfer functions for reflector and condenser plate have been incorporated into both the one-region and multi-region models discussed previously. The stability plots are shown below. Figures 15 through 18 present those for the one region model. Figures 19 through 22 present those for the multi-region model.

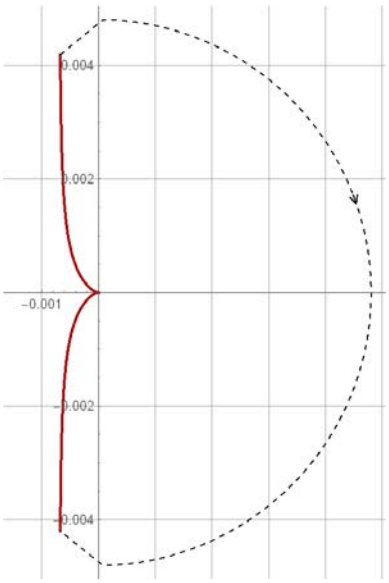

Figure 15 Single Region Extended Core Nyquist Plot

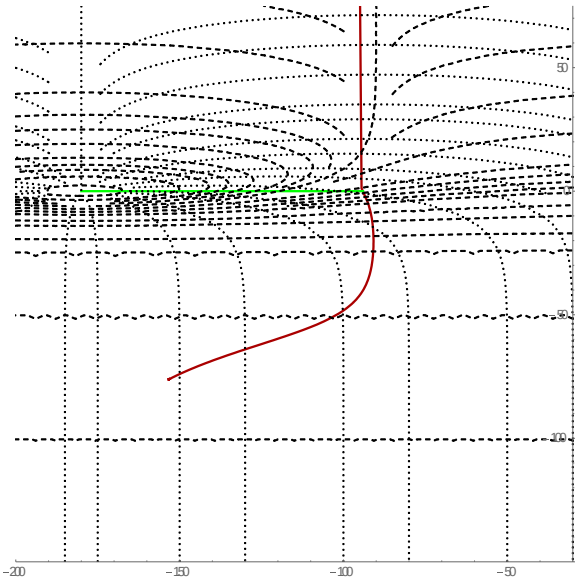

Figure 16 Single Region Extended Core Nichols Plot

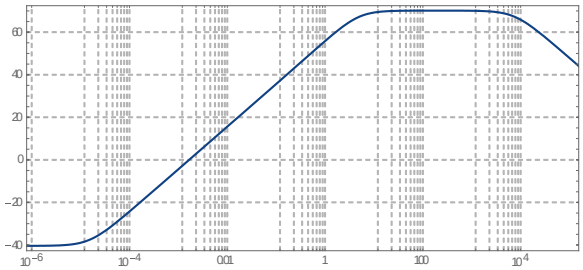

Figure 17 Single Region Extended Core Bode Amplitude Plot

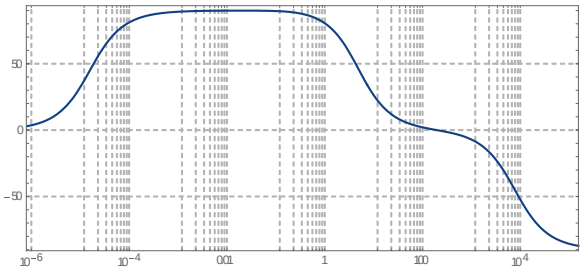

Figure 18 Single Region Extended Core Bode Frequency Plot

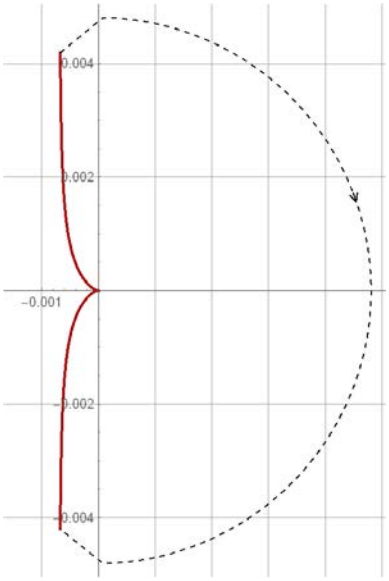

Figure 19 Multi-Region Extended Core Nyquist Plot

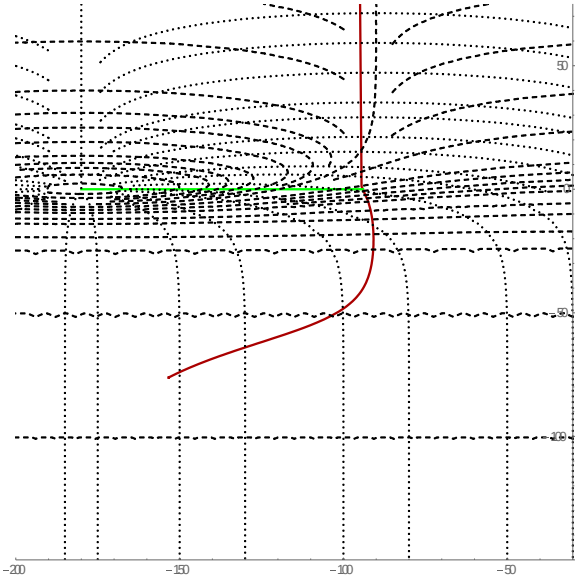

Figure 20 Multi-Region Extended Core Nichols Plot

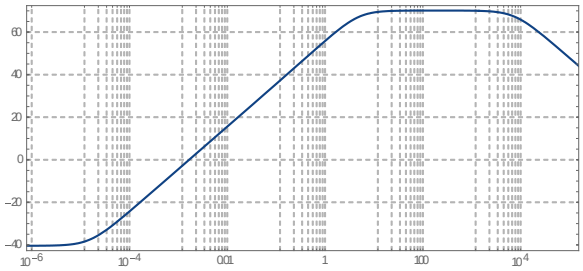

Figure 21 Multi-Region Extended Core Bode Amplitude Plot

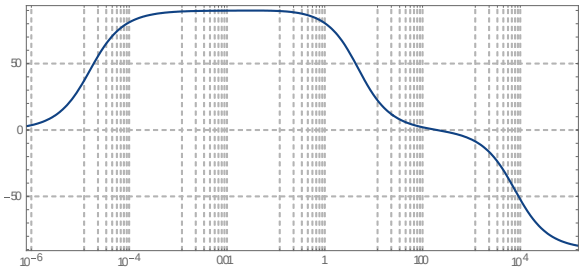

Figure 22 Multi-Region Extended Core Bode Frequency Plot

As in the previous cases, which did not include the reflector and condenser plate, the agreement between results for single region and multi-region cases can be seen. While the Nyquist and Nichols plots and suggest similar phase stability margins the Bode plots exhibit broader resonances in the extended core case. Table 2 provides the full (non-zero) poles of the open loop transfer function for the multi-region extended core:

Table 2 Poles of the multi region core open loop transfer function

(7,718.08)	(1,130.09)	(27.91)	(6.8327)	(2.8982)	(1.0241)	(0.4853)	(0.4848)	(0.4664)	(0.3633)
(0.3629)	(0.3629)	(0.3627)	(0.3613)	(0.3579)	(0.3520)	(0.3409)	(0.3401)	(0.3386)	(0.3385)
(0.3380)	(0.3318)	(0.3191)	(0.3178)	(0.3063)	(0.3043)	(0.3041)	(0.3030)	(0.2991)	(0.2902)
(0.2674)	(0.2670)	(0.2667)	(0.2665)	(0.2658)	(0.2637)	(0.2624)	(0.2448)	(0.2422)	(0.2361)
(0.2353)	(0.2284)	(0.2258)	(0.2232)	(0.2209)	(0.2173)	(0.2160)	(0.2050)	(0.1971)	(0.1964)
(0.1950)	(0.1948)	(0.1944)	(0.1942)	(0.1875)	(0.1819)	(0.1782)	(0.1755)	(0.1750)	(0.1749)
(0.1749)	(0.0682)	(0.0143)	(0.0107)	-1.58E-05					

These results illustrate that when the reflector or the condenser plate are included in model and linear stability analysis performed the results are the same as in the previous case where these components are not included.

Conclusions and Recommendations

A dynamic system simulation (DSS) has been developed to describe the expected transient behavior of the KRUSTY power reactor experiment. The current model is characterized as a physics model in that it has been developed from fundamental principles and correlations of similar components from literature. The model shows typical behavior that is expected of a core of the KRUSTY configuration cooled by heat pipes and Stirling engines. The conclusion of unconditional stability in the linear approximation and compliance with the criterion of nonlinear stability may be considered to be generally true with the understanding that “stability” in this context implies that the system is not expected to exhibit an unbounded response to a bounded event.

Uncertainties in the DSS have been described. These uncertainties arise from a lack of data on the major elements of the KRUSTY reactor including the nuclear, heat pipe, and Stirling engine subsystems. Experiments currently planned are expected to provide this data to allow the model to be refined to the point where it may be used with confidence to plan the KRUSTY experiment and provide operator the procedural information necessary to actually conduct the experiment.